CHAPTER

Shallow-Water Problems* 10

10.1 Introduction

The flow of water in shallow layers such as the ones that occur in coastal estuaries, oceans, rivers, etc., is of obvious practical importance. The prediction of tidal currents and elevations is vital for navigation and for the determination of pollutant dispersal which, unfortunately, is still frequently deposited there. The transport of sediments associated with such flows and algal growth and transport are other fields of interest.

If the free surface flow is confined to relatively thin layers the horizontal velocities are of primary importance and the problem can be reasonably approximated in two dimensions. Here we find that the resulting equations, which include in addition to the horizontal velocities the free surface elevation, can once again be written in the same conservation form as the Euler equations studied in previous chapters.

Indeed, the detailed form of these equations bears a striking similarity to that of compressible gas flow—despite the fact that now a purely incompressible fluid (water) is considered. It follows therefore that:

1. The methods developed in the previous chapters are in general applicable.
2. The type of phenomena (e.g., shocks, etc.) which we have encountered in compressible gas flows can occur again.

It will of course be found that practical interest focuses on different aspects. The objective of this chapter is therefore to introduce the basis of the derivation of the equation and to illustrate the numerical approximation techniques by a series of examples.

The approximations made in the formulation of the flow in shallow-water bodies are similar in essence to those describing the flow of air in the earth's environment and hence are widely used in meteorology. Here the vital subject of weather prediction involves their daily solution and a very large amount of computation. The interested reader will find much of the background in standard texts dealing with the subject, e.g., Refs. [1] and [2].

A particular area of interest occurs in the linearized version of the shallow-water equations which, in periodic response, are similar to those describing acoustic

*Contributed partly by P. Ortiz, Professor, University of Granada, Spain.

Finite Element Meth Fluid Dynam 7E, Volume 3. http://dx.doi.org/10.1016/B978-1-85617-635-4.00010-8

phenomena. In the next chapter we shall therefore discuss some of these periodic phenomena involved in the action and forces due to waves [3].

10.2 The basis of the shallow-water equations

In previous chapters we have introduced the essential Navier-Stokes equations and presented their incompressible, isothermal form, which we repeat below assuming full incompressibility. We now have the equation of mass conservation

$$\frac{\partial u_i}{\partial x_i} = 0 \tag{10.1a}$$

and the equation of momentum conservation

$$\frac{\partial u_j}{\partial t} + \frac{\partial}{\partial x_i}(u_i u_j) + \frac{1}{\rho}\frac{\partial p}{\partial x_j} - \frac{1}{\rho}\frac{\partial}{\partial x_i}\tau_{ij} - g_j = 0 \tag{10.1b}$$

with i, j being 1, 2, 3.

In the case of shallow-water flow, which we illustrate in Fig. 10.1 and where the direction x_3 is vertical, the vertical velocity u_3 is small, and the corresponding accelerations are negligible. The momentum equation in the vertical direction can

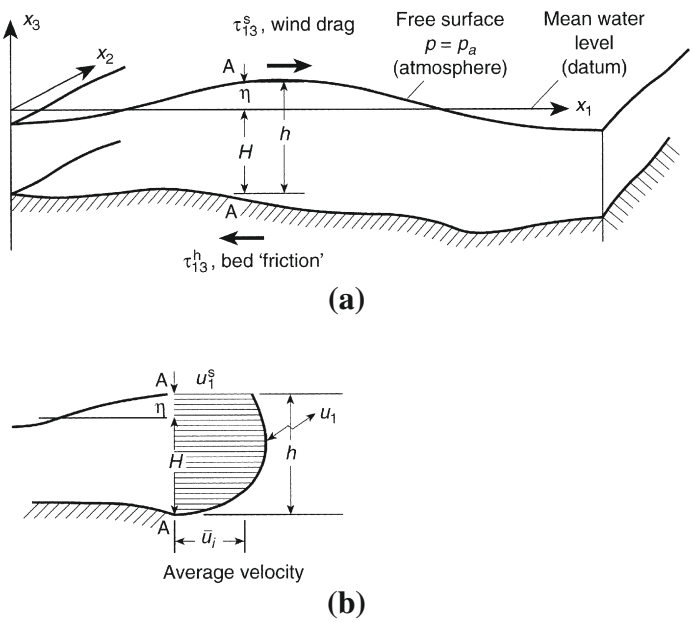

FIGURE 10.1
The shallow-water problem. Notation: (a) coordinates; (b) velocity distribution.

therefore be reduced to

$$\frac{1}{\rho}\frac{\partial p}{\partial x_3} + g = 0 \tag{10.2}$$

where $g_3 = -g$ is the gravity acceleration. After integration this yields

$$p = \rho g(\eta - x_3) + p_a \tag{10.3}$$

as, when $x_3 = \eta$, the pressure is atmospheric (p_a) (which may on occasion not be constant over the body of the water and can thus influence its motion).

On the free surface the vertical velocity u_3 can of course be related to the total time derivative of the surface elevation as discussed in Chapter 6.

With reference to Fig. 10.1 we can directly derive the depth-averaged conservation of mass equation by considering an infinitesimal control volume in the horizontal plane as

$$\frac{\partial h}{\partial t} + \frac{\partial (h\overline{u_i})}{\partial x_i} = 0 \tag{10.4}$$

where $\overline{u_i}$ is the averaged velocity field. We can immediately see the similarity with the conservation of mass equation for compressible gas flows with h replacing density ρ here. It should be noted that Eq. (10.4) can also be derived by integrating Eq. (10.1a) between $-H$ and η (see Fig. 10.1) [4].

Now we shall perform depth integration on the momentum equations in the horizontal directions, which results in depth-averaged momentum equations. We integrate Eq. (10.6) between the top and bottom surfaces, i.e.,

$$\int_{-H}^{\eta} \left[\frac{\partial u_i}{\partial t} + \frac{\partial}{\partial x_j}(u_i u_j) + \frac{1}{\rho}\frac{\partial p}{\partial x_i} - \frac{1}{\rho}\frac{\partial \tau_{ij}}{\partial x_i} - f_i \right] \mathrm{d}x_3 = 0 \tag{10.5}$$

with $i = 1, 2$ and where f_i in the above equations are Coriolis accelerations. In order to integrate the above equation, we need to use the following integration formula:

$$\int_a^b \frac{\partial}{\partial s} F(r,s)dr = \frac{\partial}{\partial s}\int_a^b F(r,s)dr - F(b,s)\frac{\partial b}{\partial s} + F(a,s)\frac{\partial a}{\partial s} \tag{10.6}$$

A simple example of using the above formula is

$$\int_{-H}^{\eta} \frac{1}{\rho}\frac{\partial p}{\partial x_i} dx_3 = \frac{\partial}{\partial x_i}\int_{-H}^{\eta} \frac{p}{\rho} dx_3 - \left[\frac{p}{\rho}\right]_{\eta}\left(\frac{\partial \eta}{\partial x_i}\right) + \left[\frac{p}{\rho}\right]_{-H}\left(-\frac{\partial H}{\partial x_i}\right) \tag{10.7}$$

After integration the depth-averaged momentum Eq. (10.5) becomes (substituting Eq.10.3)

$$\frac{\partial h\overline{u_i}}{\partial t} + \frac{\partial h\overline{u_i u_j}}{\partial x_j} = -gh\frac{\partial \eta}{\partial x_i} + \frac{1}{\rho}(\tau_{3i}^s - \tau_{3i}^b) + hf_i - \frac{h}{\rho}\frac{\partial p_a}{\partial x_i} + \frac{1}{\rho}\frac{\partial}{\partial x_j}\int_{-H}^{\eta} \tau_{ij}\, dx_3 \tag{10.8}$$

where superscripts s and b respectively indicate top and bottom (seafloor) surfaces. In Eq. (10.8) the shear stresses on the surface can be prescribed externally, given,

say, the wind drag. The bottom shear is frequently expressed by suitable hydraulic resistance formulae, e.g., the Chézy expression, giving

$$\tau_{3i}^{\mathrm{b}} = \frac{\rho g |\bar{\mathbf{u}}| \bar{u}_i}{C h^2} \tag{10.9}$$

where

$$|\bar{\mathbf{u}}| = \sqrt{\bar{u}_i \bar{u}_i}, \qquad i = 1, 2$$

and C is the Chézy coefficient. The Coriolis accelerations, f_i, in Eq. (10.8) are important in large-scale problems and defined as

$$f_1 = \hat{f}\bar{u}_2 \qquad f_2 = -\hat{f}\bar{u}_1 \tag{10.10}$$

where $\hat{f}$ is the Coriolis parameter. At this stage we omit the stresses acting within the fluid and simply consider the surface and base drag, which can be evaluated independently. The addition of shear stresses on vertical faces of the slice can be included but are neglected in this book. Thus, the simplified momentum equation without the fluid stress terms is

$$\frac{\partial h\overline{u_i}}{\partial t} + \frac{\partial h\overline{u_i u_j}}{\partial x_j} = -gh\frac{\partial \eta}{\partial x_i} + \frac{1}{\rho}(\tau_{3i}^{s} - \tau_{3i}^{b}) + hf_i - \frac{h}{\rho}\frac{\partial p_a}{\partial x_i} \tag{10.11}$$

If we compare the above equation with the Euler equations for compressible gas flows we find the equivalent pressure term in Eq. (10.11) appears in its non-conservation form. Also, an additional variable η is introduced. In order to write the above equation in conservation form and to eliminate the additional variable η, let us consider the following alternative form of the equivalent pressure term with $\eta = h - H$:

$$-gh\frac{\partial \eta}{\partial x_i} = -\frac{\partial}{\partial x_i}\left(g\frac{h^2 - H^2}{2}\right) + g(h - H)\frac{\partial H}{\partial x_i} \tag{10.12}$$

Substituting the above alternative form into Eq. (10.11) gives

$$\frac{\partial (h\bar{u}_i)}{\partial t} + \frac{\partial}{\partial x_j}\left(h\bar{u}_i\bar{u}_j\right) = -\frac{\partial}{\partial x_i}\left[\frac{1}{2}g(h^2 - H^2)\right] + \frac{1}{\rho}(\tau_{3i}^{\mathrm{s}} - \tau_{3i}^{\mathrm{b}}) + hf_i + g(h - H)\frac{\partial H}{\partial x_i} - \frac{h}{\rho}\frac{\partial p_a}{\partial x_i} \tag{10.13}$$

Now the above equation is in a form identical to that of inviscid compressible momentum equations with h replacing ρ. The first three terms in the above equations represent transient, convection, and equivalent pressure terms. All the remaining four terms can be assumed to be source terms.

Equations (10.4) and (10.13) form the shallow-water problem. These equations may be rewritten in a compact form as

$$\frac{\partial \mathbf{\Phi}}{\partial t} + \frac{\partial \mathbf{F_i}}{\partial x_i} + \mathbf{Q} = 0 \tag{10.14}$$

where

$$\mathbf{\Phi} = \begin{Bmatrix} h \\ h\bar{u}_1 \\ h\bar{u}_2 \end{Bmatrix} \tag{10.15a}$$

$$\mathbf{F}_i = \begin{Bmatrix} h\bar{u}_i \\ h\bar{u}_1\bar{u}_i + \delta_{1i}\frac{1}{2}g(h^2 - H^2) \\ h\bar{u}_2\bar{u}_i + \delta_{2i}\frac{1}{2}g(h^2 - H^2) \end{Bmatrix} \tag{10.15b}$$

and

$$\mathbf{Q} = \begin{Bmatrix} 0 \\ -h\hat{f}\bar{u}_2 - g(h-H)\dfrac{\partial H}{\partial x_1} + \dfrac{h}{\rho}\dfrac{\partial p_a}{\partial x_1} - \dfrac{1}{\rho}\tau^{\mathrm{s}}_{31} + \dfrac{g\bar{u}_1|\bar{\mathbf{u}}|}{Ch^2} \\ h\hat{f}\bar{u}_1 - g(h-H)\dfrac{\partial H}{\partial x_2} + \dfrac{h}{\rho}\dfrac{\partial p_a}{\partial x_2} - \dfrac{1}{\rho}\tau^{\mathrm{s}}_{32} + \dfrac{g\bar{u}_2|\bar{\mathbf{u}}|}{Ch^2} \end{Bmatrix} \tag{10.15c}$$

with $i = 1, 2$.

The above, conservative, form of shallow-water equations was first presented in Refs. [4] and [5] and is generally applicable. However, many variants of the general shallow-water equations exist in the literature, introducing various approximations.

In the following sections of this chapter we shall discuss time-stepping solutions of the full set of the above equations in transient situations and in corresponding steady-state applications.

If we deal with the linearized form of Eqs. (10.4) and (10.13), we see immediately that on omission of all nonlinear terms, bottom drag, etc., and taking $h \sim H$, we can write these equations as

$$\frac{\partial h}{\partial t} + \frac{\partial}{\partial x_i}(H\bar{u}_i) = 0 \tag{10.16a}$$

$$\frac{\partial (H\bar{u}_i)}{\partial t} + gH\frac{\partial}{\partial x_i}(h - H) = 0 \tag{10.16b}$$

Noting that

$$\eta = h - H \qquad \text{and} \qquad \frac{\partial h}{\partial t} = \frac{\partial \eta}{\partial t}$$

the above becomes

$$\frac{\partial \eta}{\partial t} + \frac{\partial}{\partial x_i}(H\bar{u}_i) = 0 \tag{10.17a}$$

$$\frac{\partial (H\bar{u}_i)}{\partial t} + gH\frac{\partial \eta}{\partial x_i} = 0 \tag{10.17b}$$

Elimination of $H\bar{u}_i$ immediately yields

$$\frac{\partial^2 \eta}{\partial t^2} - \frac{\partial}{\partial x_i}\left(gH\frac{\partial \eta}{\partial x_i}\right) = 0 \tag{10.18}$$

or the standard Helmholtz wave equation. For this, many special solutions are analyzed in the next chapter.

The shallow-water equations derived in this section consider only the depth-averaged flows and hence cannot reproduce certain phenomena that occur in nature and in which some velocity variation with depth has to be allowed for. In many such problems the basic assumption of a vertically hydrostatic pressure distribution is still valid and a form of shallow-water behavior can be assumed.

The extension of the formulation can be achieved by an *a priori* division of the flow into strata in each of which different velocities occur. The final set of discretized equations consists then of several, coupled, two-dimensional approximations. Alternatively, the same effect can be introduced by using several different velocity "trial functions" for the vertical distribution, as was suggested by Zienkiewicz and Heinrich [6]. Such generalizations are useful but outside the scope of the present text.

10.3 Numerical approximation

Both finite difference and finite element procedures have for many years been used widely in solving the shallow-water equations. The latter approximation has been applied in the 1980s and Kawahara [7] and Navon [8] survey the early applications to coastal and oceanographic engineering. In most of these the standard procedures of spatial discretization followed by suitable time-stepping schemes are adopted [9–16]. In meteorology the first application of the finite element method dates back to 1972, as reported in the survey given in Ref. [17], and the range of applications has been increasing steadily [4,5,18–57].

At this stage the reader may well observe that with the exception of source terms, the isothermal compressible flow equations can be transformed into the depth integrated shallow-water equations with the variables being changed as follows:

$$\begin{aligned} \rho \text{ (density)} &\rightarrow h \text{ (depth)} \\ u_i \text{ (velocity)} &\rightarrow \bar{u}_i \text{ (mean velocity)} \\ p \text{ (velocity)} &\rightarrow \frac{1}{2} g(h^2 - H^2) \end{aligned}$$

These similarities suggest that the characteristic-based-split (CBS) algorithm adopted in the previous chapters for compressible flows be used for the shallow-water equations [58].

By using the Cartesian system and notation of the Fig. 10.1 the shallow-water equations can now be rewritten in a convenient form for the general CBS formulation developed in Chapter 3, as

$$\frac{\partial h}{\partial t} + \frac{\partial U_i}{\partial x_i} = 0$$

$$\frac{\partial U_i}{\partial t} + \frac{\partial (\overline{u}_j U_i)}{\partial x_j} + \frac{\partial}{\partial x_i}\left[\frac{1}{2} g(h^2 - H^2)\right] + Q_i = 0$$

where $U_i = h\bar{u}_i$. The rest of the variables are the same as described before. The extension of effective finite element solutions of high-speed flows to shallow-water problems has already been successful in the case of the Taylor-Galerkin method [4,5,48]. However, the semi-implicit form of the general CBS formulation provides a critical time step dependent only on the current velocity of the flow **U** (for pure convection),

$$\Delta t \leq \frac{d}{|\mathbf{U}|} \tag{10.19}$$

where d is the element size, instead of a critical time step in terms of the wave celerity $c = \sqrt{gh}$,

$$\Delta t \leq \frac{d}{c + |\mathbf{U}|} \tag{10.20}$$

which places a severe contraint on fully explicit methods such as the Taylor-Galerkin approximation and others [4,5,32] particularly for the analysis of long-wave propagation in shallow waters and in general for low Froude number problems.

Important savings in computation can be reached in these situations obtaining for some practical cases up to 20 times the critical (explicit) time step, without seriously affecting the accuracy of the results. When nearly critical to supercritical flows must be studied, the fully explicit form is recovered, and the results observed for these cases are also excellent [59,60]. The three essential steps of the CBS scheme may be written in its semi-discrete form as

Step 1:

$$\Delta U_i^\star = \Delta t \left[-\frac{\partial}{\partial x_j}(u_j U_i) - Q_i + \frac{\Delta t}{2} u_k \frac{\partial}{\partial x_k}\left(\frac{\partial}{\partial x_j}(u_j U_i) + Q_i \right) \right]^n \tag{10.21}$$

Step 2:

$$\Delta h = -\Delta t \left[\frac{\partial U_i^n}{\partial x_i} + \theta_1 \frac{\partial \Delta U_i^\star}{\partial x_i} - \Delta t \theta_1 \left(\frac{\partial^2 p^n}{\partial x_i \partial x_i} + \theta_2 \frac{\partial^2 \Delta p}{\partial x_i \partial x_i} \right) \right] \tag{10.22}$$

Step 3:

$$\Delta U_i = U_i^{n+1} - U_i^n = \Delta U_i^* - \Delta t \frac{\partial p^{n+\theta_2}}{\partial x_i} + \frac{\Delta t^2}{2} u_k \frac{\partial^2 p^n}{\partial x_k \partial x_i} \tag{10.23}$$

with $p = g(h^2 - H^2)/2$. In the above equations, $0.5 \geq \theta_1 \geq 1.0$ and $\theta_2 = 0$ for explicit scheme and $0.5 \geq \theta_1 \geq 1.0$ and $0.5 \geq \theta_2 \geq 1.0$ for semi-implicit scheme. For further details on the time and spatial discretizations, the readers are referred to Chapter 3.

In the examples that follow we shall illustrate several problems solved by the CBS procedure, and with the Taylor-Galerkin method.

10.4 Examples of application

10.4.1 Transient one-dimensional problems: A performance assessment

In this section we present some relatively simple examples in one space dimension to illustrate the applicability of the algorithms.

Example 10.1. Solitary wave

The first, illustrated in Fig. 10.2, shows the progress of a solitary wave [61] onto a shelving beach. This frequently studied situation [62,63] shows well the progressive steepening of the wave often obscured by schemes that are very dissipative.

Example 10.2. Dam break

The second example, illustrated in Fig. 10.3, illustrates the so-called "dam break" problem diagrammatically. Here a dam separating two stationary water levels is suddenly removed and the almost vertical waves progress into the two domains. This problem, somewhat similar to those of a shock tube in compressible flow, has been solved quite successfully even without artificial diffusivity.

Example 10.3. Bore

The final example of this section, Fig. 10.4, shows the formation of an idealized "bore" or a steep wave progressing into a channel carrying water at a uniform speed caused by a gradual increase of the downstream water level. Despite the fact that the flow speed is "subcritical" (i.e., velocity $< \sqrt{gh}$), a progressively steepening, traveling shock clearly develops.

10.4.2 Two-dimensional periodic tidal motions

The extension of the computation into two space dimensions follows the same pattern as that described in compressible formulations. Again linear triangles are used to interpolate the values of h, hu_1, and hu_2. The main difference in the solutions is that of emphasis.

Example 10.4. Periodic wave

The first example of Fig. 10.5 is presented merely as a test problem. Here the frictional resistance is linearized and an exact solution known for a periodic response [64] is used for comparison. This periodic response is obtained numerically by performing five cycles with the input boundary conditions. Although the problem is essentially one-dimensional, a two-dimensional uniform mesh was used and the agreement with analytical results is found to be quite remarkable.

Example 10.5. Bristol channel

In the second example we enter the domain of more realistic applications [4,5,58–60,65]. Here the "test bed" is provided by the Bristol Channel and the Severn Estuary,

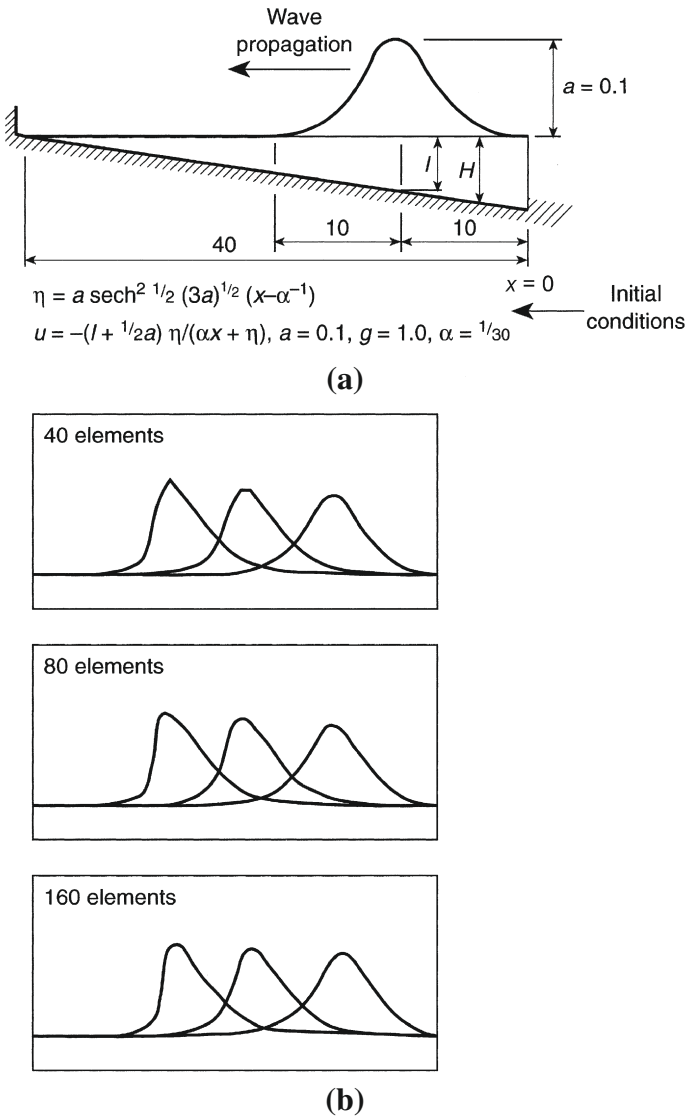

FIGURE 10.2
Shoaling of a wave: (a) problem statement; (b) solution, for 40, 80, and 160 elements at various times.

known for some of the highest tidal motions in the world. Figure 10.6 shows the location and the scale of the problem.

The objective is here to determine tidal elevations and currents currently existing (as a possible preliminary to a subsequent study of the influence of a barrage which

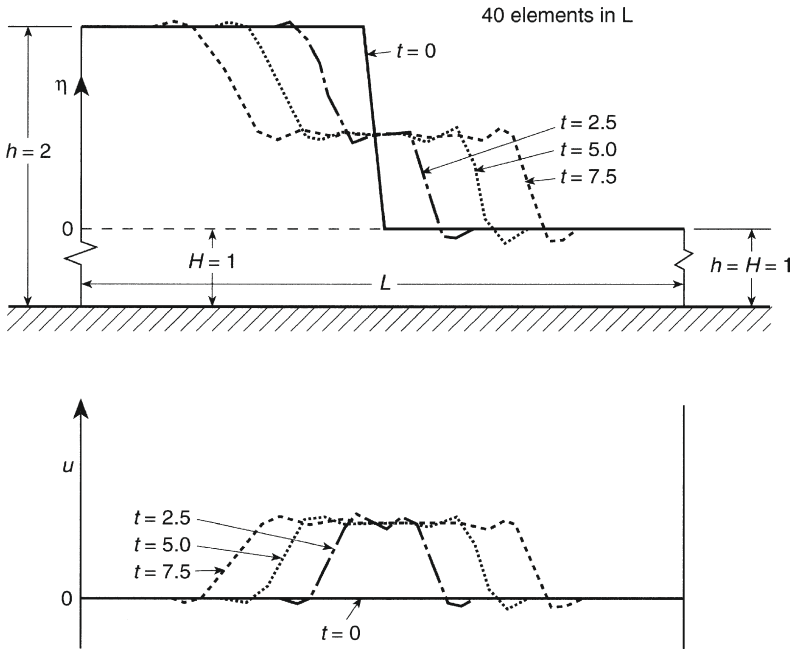

FIGURE 10.3

Propagation of waves due to dam break ($C_{\text{Lap}} = 0$). Forty elements in analysis domain. $C = \sqrt{gH} = 1$, $\Delta t = 0.25$.

some day may be built to harness the tidal energy). Before commencement of the analysis the extent of the analysis domain must be determined by an arbitrary, seaward, boundary. On this the measured tidal heights will be imposed.

This height-prescribed boundary condition is not globally conservative and can produce undesired reflections. These effects sometimes lead to considerable errors in the calculations, particularly if long-term computations are to be carried out (like, for instance, in some pollutant dispersion analysis). For these cases, more general open boundary conditions can be applied, as, for example, those described in Refs. [35] and [36].

The analysis was carried out on four meshes of linear triangles shown in Fig. 10.7. These meshes encompass two positions of the external boundary and it was found that the differences in the results obtained by four separate analyses were insignificant.

The mesh sizes ranged from 2 to 5 km in minimum size for the fine and coarse subdivisions. The average depth is approximately 50 m but of course full bathygraphy information was used with depths assigned to each nodal point.

The numerical study of the Bristol Channel was completed by a comparison of performance between the explicit and semi-explicit algorithms [59]. The results for the coarse mesh were compared with measurements obtained by the Institute of Oceanographic Science (IOS) for the M_2 tide [65], with time steps corresponding to the critical

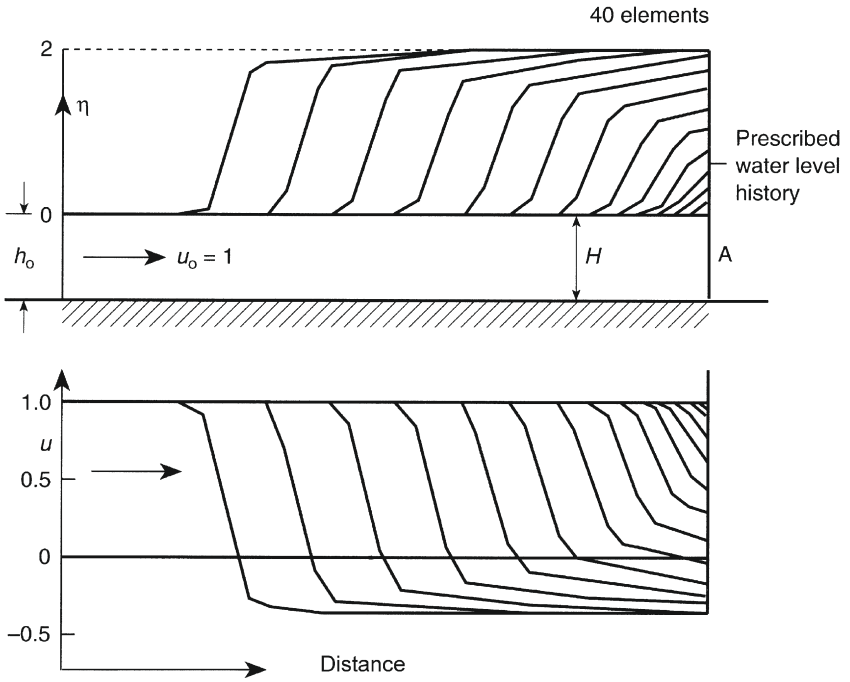

FIGURE 10.4
A "bore" created in a stream due to water level rise downstream (A). Level at A, $\eta = 1 - \cos \pi t/30$ $(0 \leq t \leq 30)$, 2 $(30 \leq t)$. Levels and velocities at intervals of 5 time units, $\Delta t = 0.5$.

(explicit) time step (50 s), and four times (200 s) and eight times (400 s) the critical time step. A constant real friction coefficient (Manning) of 0.038 was adopted for all of the estuary. Coriolis forces were included. The analysis proved that the Coriolis effect was very important in terms of phase errors. Table 10.1 represents a comparison between observations and computations in terms of amplitudes and phases for seven different points which are represented in the location map (Fig. 10.6), for the three different time steps described above. The maximum error in amplitude only increases by 1.4% when the time step of 400 s is used with respect to the time step of 50 s, while the absolute error in phases (−13°) is two degrees more than the case of 50 s (−11°). These bounds show a remarkable accuracy for the semi-explicit model. In Fig. 10.8 the distribution of velocities at different times of the tide is illustrated (explicit model).

Example 10.6. River Severn bore

In the analysis presented we have omitted details of the River Severn upstream of the eastern limit (see Figs. 10.6 and 10.9a), where a "bore" moving up the river can be observed. An approach to this phenomenon is made by a simplified straight

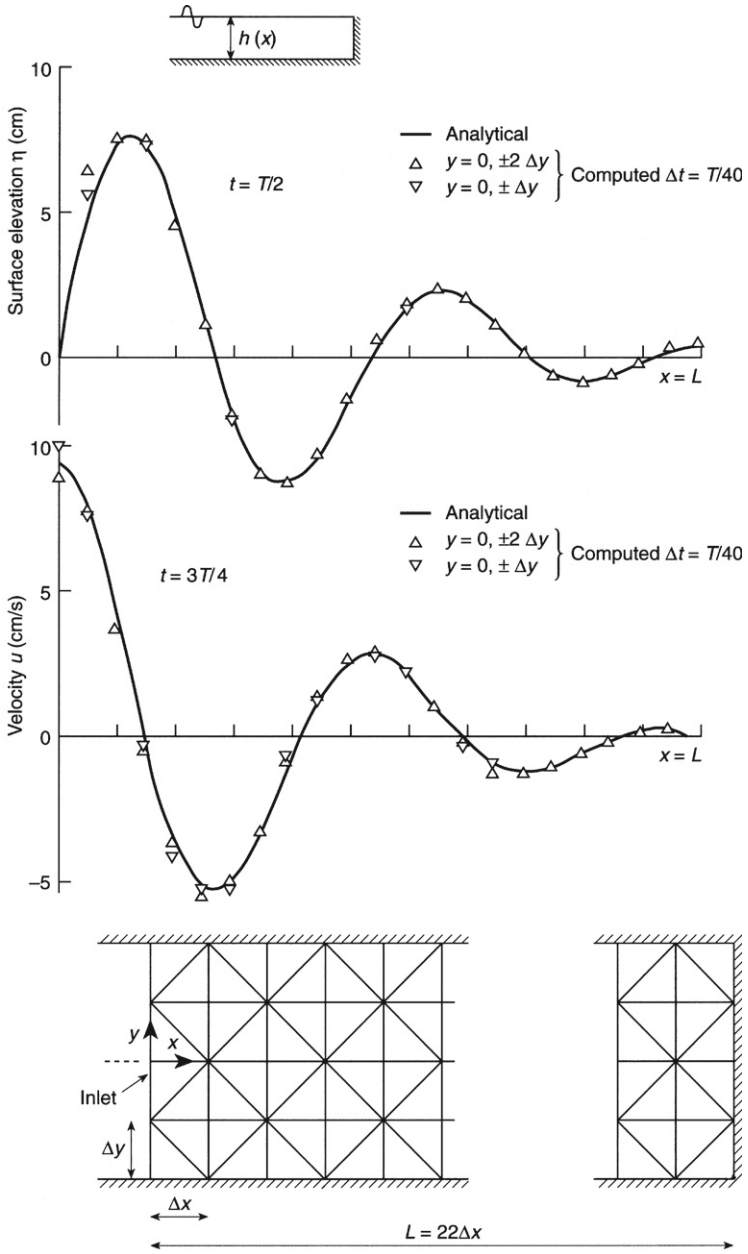

FIGURE 10.5
Steady-state oscillation in a rectangular channel due to periodic forcing of surface elevation at an inlet. Linear frictional dissipation [32].

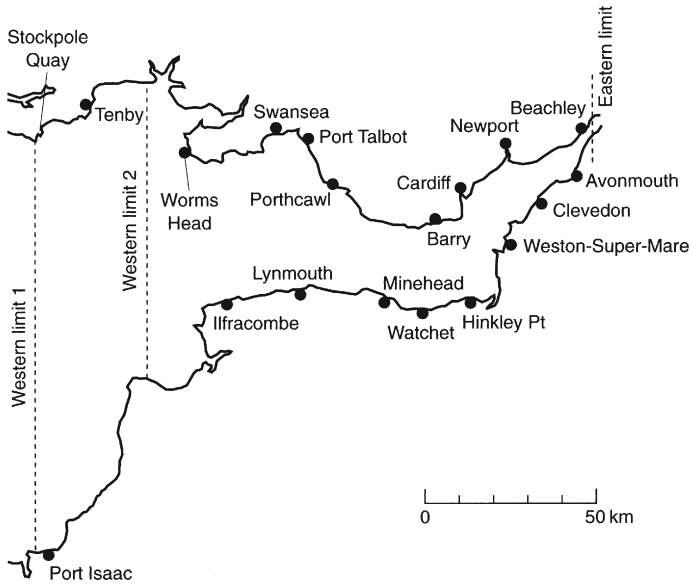

FIGURE 10.6
Location map. Bristol Channel and Severn Estuary.

extension of the mesh used previously, preserving an approximate variation of the bottom and width until the point G (Gloucester) (77.5 km from Avonmouth), but obviously neglecting the dissipation and inertia effects of the bends. Measurement points are located at B and E, and the results (elevations) are presented in Fig. 10.9d for the points A, B, and E in time, along with a steady river flow. A typical shape for a tidal bore can be observed for the point E, with fast flooding and a smooth ebbing of water. (The flooding takes place from the minimum to maximum level in less than 25 min.)

10.4.3 Tsunami waves

A problem of some considerable interest in earthquake zones is that of so-called tidal waves or tsunamis. These are caused by sudden movements in the earth's crust and can on occasion be extremely destructive. The analysis of such waves presents no difficulties in the general procedure demonstrated and indeed is computationally cheaper as only relatively short periods of time need be considered. To illustrate a typical possible tsunami wave we have created one in the Severn Estuary just analyzed (to save problems of mesh generation, etc., for another more likely configuration).

Example 10.7. Tsunami wave in Severn Estuary

Here the tsunami is forced by an instantaneous raising of an element situated near the center of the estuary by some 6 m and the previously designed mesh was used

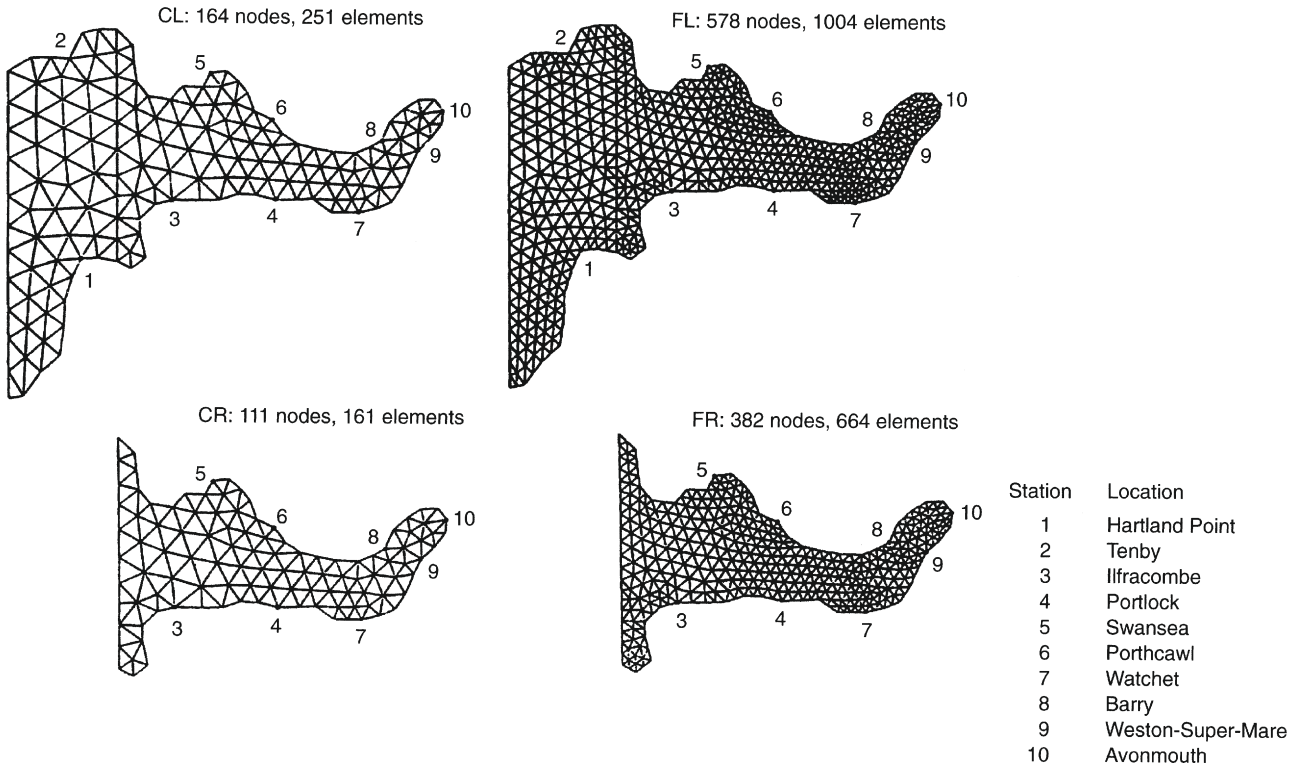

FIGURE 10.7

Finite element meshes. Bristol Channel and Severn Estuary.

Table 10.1 Bristol Channel and Severn Estuary—Observed Results and FEM Computation (FL Mesh) of Tidal Half-Amplitude ($m \times 10^2$)

Location	Observed	FEM
Tenby	262	260 (−1%)
Swansea	315	305 (−3%)
Cardiff	409	411 (0%)
Porthcawl	317	327 (+3%)
Barry	382	394 (+3%)
Port Talbot	316	316 (−1%)
Newport	413	420 (+2%)
Ilfracombe	308	288 (−6%)
Minehead	358	362 (+1%)

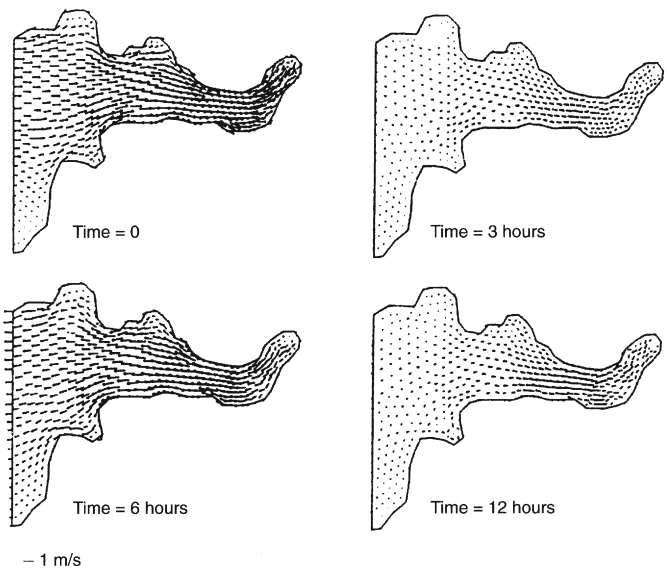

FIGURE 10.8
Velocity vector plots (FL mesh).

(FL). The progress of the wave is illustrated in Fig. 10.10. The tsunami wave was superimposed on the tide at its highest level—though of course the tidal motion was allowed for. This example was included in Ref. [5].

One particular point only needs to be mentioned in this calculation. This is the boundary condition on the seaward, arbitrary, limit. Here the Riemann decomposition of the type discussed earlier has to be made if tidal motion is to be incorporated and

note taken of the fact that the tsunami forms only an outgoing wave. This, in the absence of tides, results simply in application of the free boundary condition there.

The clean way in which the tsunami is seen to leave the domain in Fig. 10.10 testifies to the effectiveness of this process.

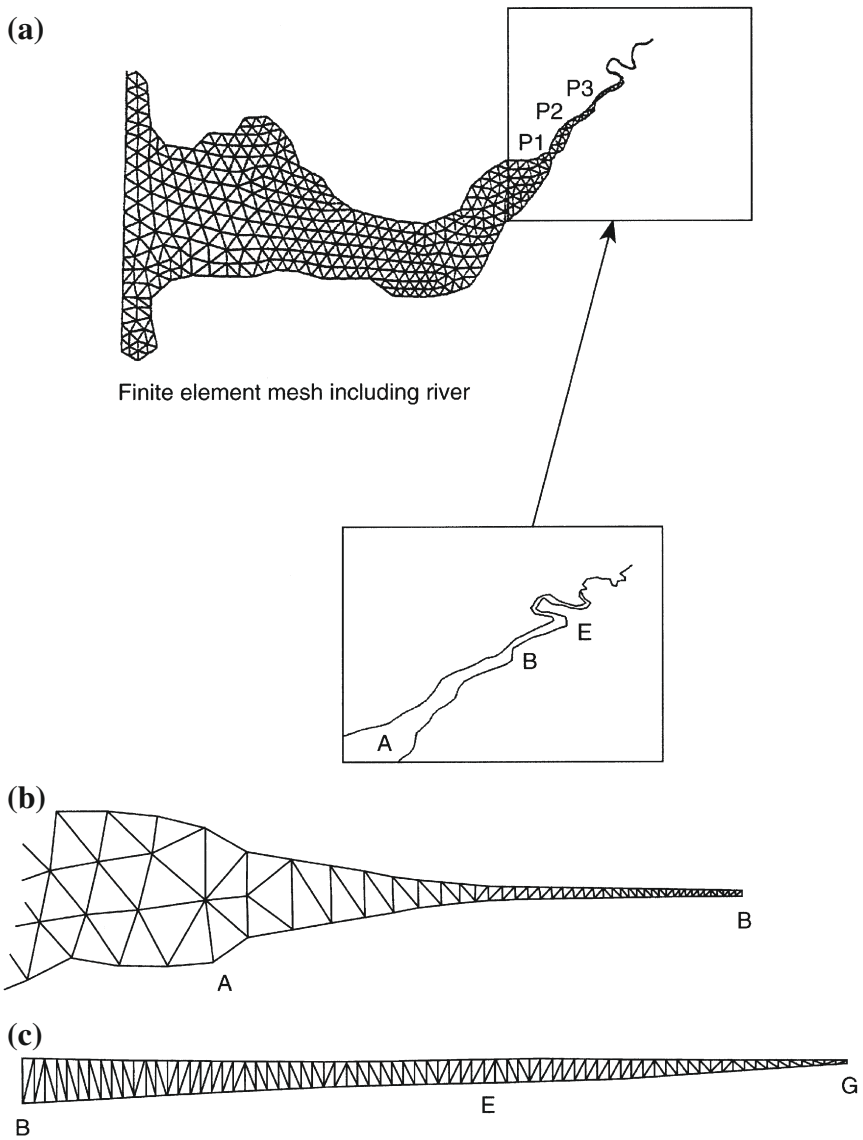

FIGURE 10.9
Finite element mesh used in the Severn bore calculations (a) Full domain (b) Part of the domain between points A and B (c) Part of the domain beyond point B.

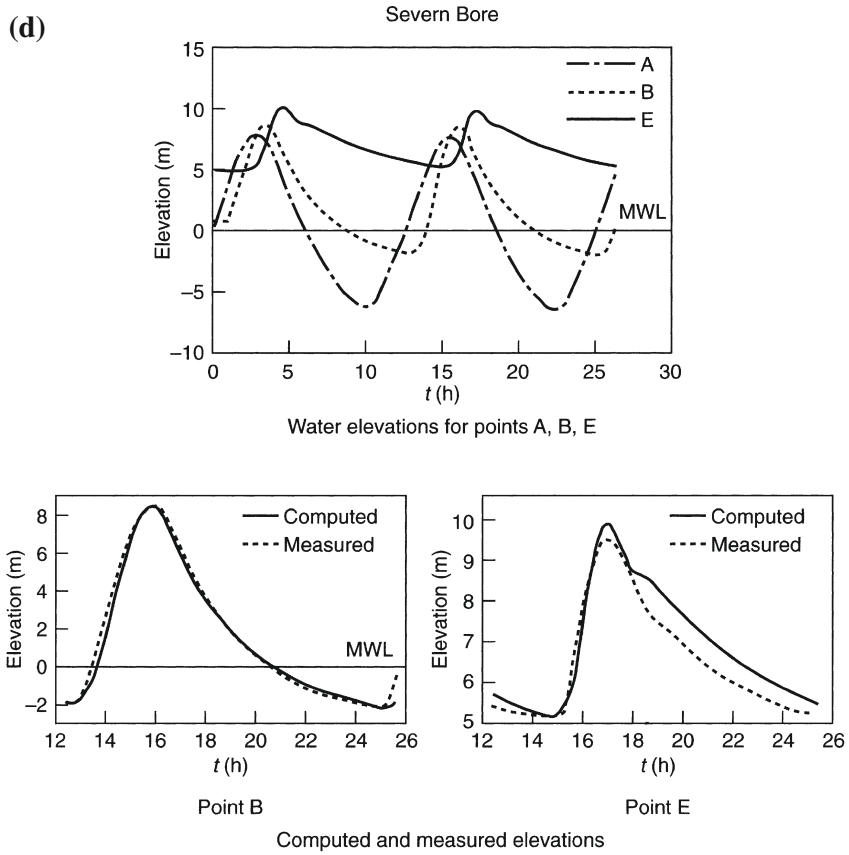

FIGURE 10.9
(Continued).

10.4.4 Steady-state solutions

On occasion steady-state currents such as the ones caused by persistent wind motion or other influences have to be considered. Here once again the transient form of explicit computation proves very effective and convergence is generally more rapid than in compressible flow as the bed friction plays a greater role. The interested reader will find many such steady-state solutions in the literature.

Example 10.8. Steady-state solution

In Fig. 10.11 we show a typical example. Here the currents are induced by the breaking of waves which occurs when these reach small depths creating so-called radiation stresses [6,30,66]. The "forces" due to breaking are the cause of longshore currents and rip currents in general. The figure illustrates this effect on a harbor.

It is of interest to remark that in the problem discussed, the side boundaries have been "repeated" to model an infinite harbor series [66].

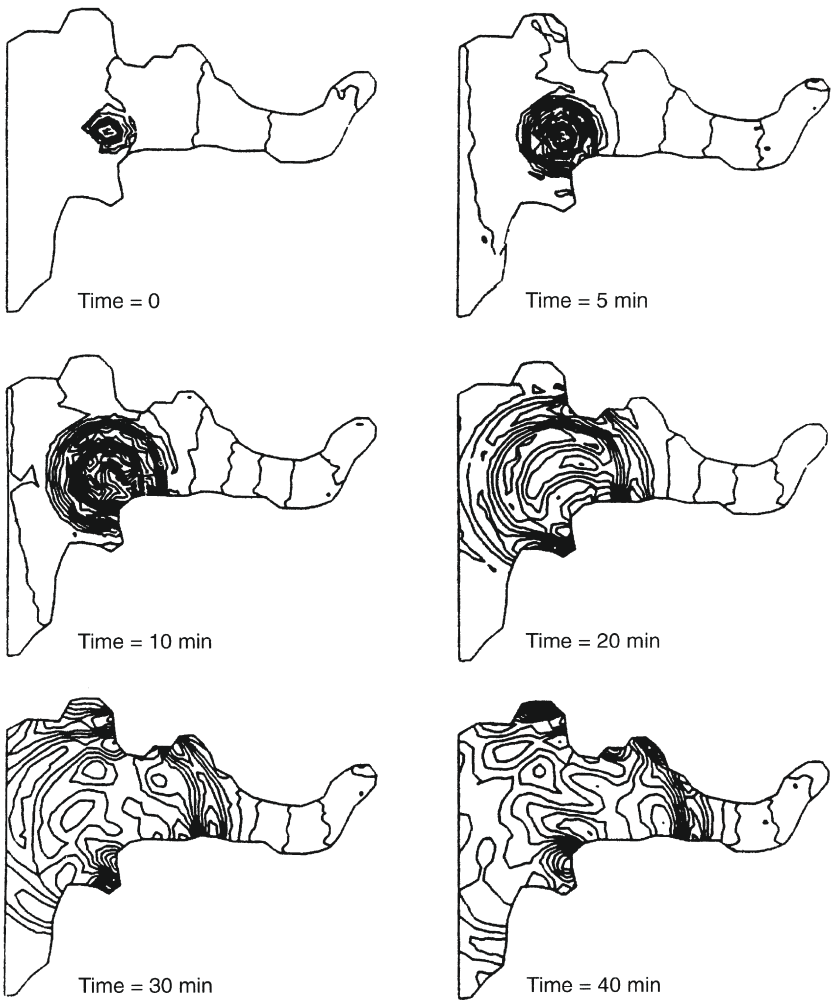

FIGURE 10.10
Severn tsunami. Generation during high tide. Water height contours (times after generation).

Example 10.9. Supercritical flow

Another type of interesting steady-state (and transient) problem concerns supercritical flows over hydraulic structures, with shock formation similar to those present in high-speed compressible flows. To illustrate this range of flows, the problem of a symmetric channel of variable width with a supercritical inflow is shown here. For a supercritical flow in a rectangular channel with a symmetric transition on both sides, a combination of a "positive" jump and "negative" waves, causing a decrease in depth, appears. The profile of the negative wave is gradual and an approximate solution

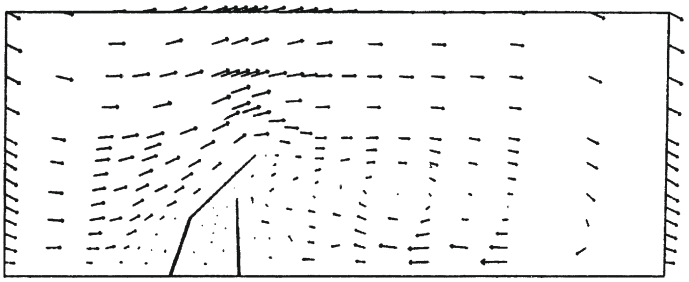

FIGURE 10.11
Wave-induced steady-state flow past a harbor [30].

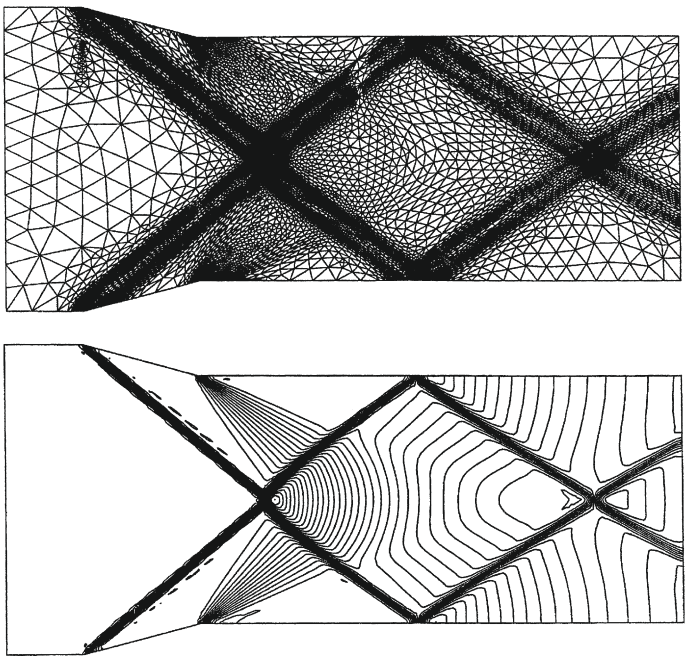

FIGURE 10.12
Supercritical flow and formation of shock waves in symmetric channel of variable width contours of h. Inflow Froude number = 2.5. Constriction: 15°.

can be obtained by assuming no energy losses and that the flow near the wall turns without separation. The constriction and enlargement analyzed here was 15°, and the final mesh used was of only 6979 nodes, after two remeshings. The supercritical flow had an inflow Froude number of 2.5 and the boundary conditions were as follows: heights and velocities prescribed in inflow (left boundary of Fig. 10.12), slip boundary on walls (upper and lower boundaries in Fig. 10.12), and free variables on the outflow boundary (right side of Fig. 10.12). The explicit version with local time

step was adopted. Figure 10.12 represents contours of heights, where "cross" waves and "negative" waves are contained. One can observe the "gradual" change in the behavior of the negative wave created at the origin of the wall enlargement.

10.5 Drying areas

A special problem encountered in transient, tidal, computations is that of boundary change due to changes of water elevation. This has been ignored in the calculation presented for the Bristol Channel-Severn Estuary as the movements of the boundary are reasonably small in the scale analyzed. However, in that example these may be of the order of 1 km and in tidal motions near Mont St. Michel, France, can reach 12 km. Clearly on some occasions such movements need to be considered in the analysis and many different procedures for dealing with the problem have been suggested. In Fig. 10.13 we show the simplest of these which is effective if the total movement can be confined to one element size. Here the boundary nodes are repositioned along the normal direction as required by elevation changes $\Delta\eta$.

If the variations are larger than those that can be absorbed in a single element some alternatives can be adopted, such as partial remeshing over layers surrounding the distorted elements or a general smooth displacement of the mesh.

10.6 Shallow-water transport

Shallow-water currents are frequently the carrier for some quantities which may disperse or decay in the process. Typical here is the transport of hot water when discharged from power stations, or of the sediment load or pollutants. The mechanism

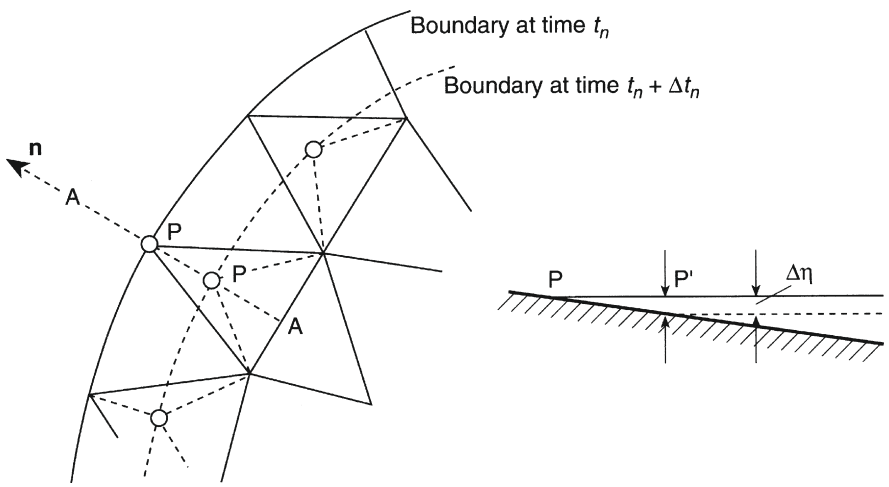

FIGURE 10.13

Adjustment of boundary due to tidal variation.

of sediment transport is quite complex [67] but in principle follows similar rules to that of the other equations. In all cases it is possible to write *depth-averaged transport equations* in which the average velocities $\bar{u}_i$ have been determined independently.

A typical averaged equation can be written—using a scalar variable (e.g., temperature (T)) as the transported quantity—as

$$\frac{\partial(hT)}{\partial t} + \frac{\partial(h\bar{u}_i T)}{\partial x_i} - \frac{\partial}{\partial x_i}\left(hk\frac{\partial T}{\partial x_i}\right) + R = 0 \quad \text{for } i = 1, 2 \tag{10.24}$$

where h and $\bar{u}_i$ are the previously defined and computed quantities, k is an appropriate diffusion coefficient, and R is a source term.

A quasi-implicit form of the general CBS algorithm can be obtained when diffusion terms are included. In this situation practical horizontal viscosity ranges (and diffusivity in the case of transport equations) can produce limiting time steps much lower than the convection limit. To circumvent this restraint, a quasi-implicit computation, requiring an implicit computation of the viscous terms, is recommended.

The application of the CBS method for any scalar transport equation is straightforward, because of the absence of the pressure gradient term. Then, the second and third steps of the method are not necessary. The computation of the scalar hT is analogous to the intermediate momentum computation, but now a new time integration parameter θ_3 is introduced for the diffusion term such that $0 \leq \theta_3 \leq 1$.

The application of the characteristic-Galerkin procedure gives the following final matrix form (neglecting terms higher than second order):

$$\left(\mathbf{M} + \theta_3 \Delta t \mathbf{D}\right) \Delta \mathbf{T} = -\Delta t[\mathbf{C}\mathbf{T}^n + \mathbf{M}\mathbf{R}^n] - \frac{\Delta t^2}{2}[\mathbf{K}_u \mathbf{T}^n + \mathbf{f}_R] - \Delta t \mathbf{D}\mathbf{T}^n + \boldsymbol{f}_{\boldsymbol{b}} \tag{10.25}$$

where now $\mathbf{T}$ is the vector of nodal hT values and we have

$$\mathbf{M} = \int_\Omega \mathbf{N}^{\mathrm{T}}\mathbf{N}\,\mathrm{d}\Omega$$

$$\mathbf{C} = \int_\Omega \mathbf{N}^{\mathrm{T}}\bar{u}_i\frac{\partial \mathbf{N}}{\partial x_j}\,\mathrm{d}\Omega$$

$$\mathbf{K}_u = \int_\Omega \frac{\partial}{\partial x_k}(\mathbf{N}^{\mathrm{T}}\bar{u}_k)\frac{\partial}{\partial x_j}(\mathbf{N}\bar{u}_j)\mathrm{d}\Omega$$

$$\mathbf{D} = \int_\Omega \frac{\partial \mathbf{N}^{\mathrm{T}}}{\partial x_i}k\frac{\partial \mathbf{N}}{\partial x_i}\,\mathrm{d}\Omega$$

$$\mathbf{f}_R = \int_\Omega \frac{\partial}{\partial x_k}(\mathbf{N}^{\mathrm{T}})\mathbf{N}\boldsymbol{R}\mathrm{d}\Omega$$

and

$$\boldsymbol{f}_{\boldsymbol{b}} = \Delta t \int_\Gamma \mathbf{N}k\frac{\partial T}{\partial x_i}\cdot n_i\,\mathrm{d}\Gamma$$

As an illustration of a real implementation, the parameters involved in the study of transport of salinity in an industrial application for a river area are considered here. The region studied was approximately 55 km long and the mean value of the eddy

diffusivity was $k = 40\ \text{ms}^{-1}$. The limiting time step for convection (considering eight components of tides) was 3.9 s. This limit was severely reduced to 0.1 s if the diffusion term was active and solved explicitly. The convective limit was recovered assuming an implicit solution with $\theta_3 = 0.5$. The comparisons of diffusion error between computations with 0.1 s and 3.9 s had a maximum diffusion error of 3.2% for the 3.9 s calculation, showing enough accuracy for engineering purposes, taking into account that the time stepping was increased 40 times, reducing dramatically the cost of computation. This reduction is fundamental when, in practical applications, the behavior of the transported quantity must be computed for long-term periods, as was this problem, where the evolution of the salinity needed to be calculated for more than 60 periods of equivalent M_2 tides and for very different initial conditions. The boundary conditions are the same as for tidal problems: a partially closed region with an open boundary condition where the tide components are imposed. For this case a radiation condition based on Riemmann invariants has been used. The reader can find a detailed description in Ref. [35]. For the salinity transport equation, the open boundary condition also can be derived on the basis of Riemmann invariants in a similar way as for the rest of the equations.

In Fig. 10.14 we show by way of an example the dispersion of a *continuous* hot water discharge in an area of the Severn Estuary. Here we note not only the convection movement but also the diffusion of the temperature contours.

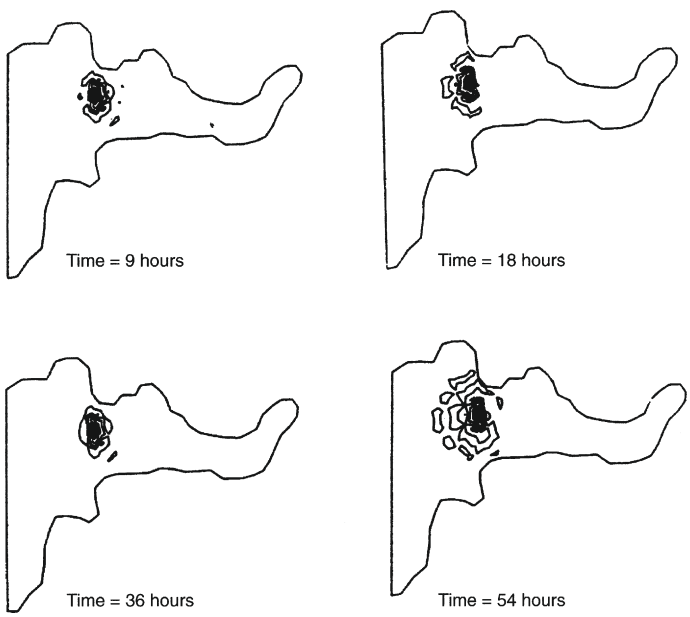

FIGURE 10.14
Heat convection and diffusion in tidal currents. Temperature contours at several times after discharge of hot fluid.

10.7 Concluding remarks

In this chapter we summarized another important form of incompressible fluid dynamics equations to solve shallow-water flows. The important features of various numerical solution procedures are also mentioned here. Turbulent fluid dynamics and accurate estimation of free surface in estuaries are a growing area of research but much more complicated approaches are necessary to tackle such problems. However, the procedure explained in this chapter, though it has limitations, is easy to follow and very effective in getting a quick solution to shallow-water problems.

References

[1] M.B. Abbott, Computational Hydraulics. Elements of the Theory of Free Surface Flows, Pitman, London, 1979.
[2] G.J. Haltiner, R.T. Williams, Numerical Prediction and Dynamic Meteorology, Wiley, New York, 1980.
[3] O.C. Zienkiewicz, R.W. Lewis, K.G. Stagg, Numerical Methods in Offshore Engineering, Wiley, Chichester, 1978.
[4] J. Peraire, A finite method for convection dominated flows, Ph.D. Thesis, University of Wales, Swansea, 1986.
[5] J. Peraire, O.C. Zienkiewicz, K. Morgan, Shallow water problems: a general explicit formulation, Int. J. Numer. Methods Eng. 22 (1986) 547–574.
[6] O.C. Zienkiewicz, J.C. Heinrich, A unified treatment of steady state shallow water and two dimensional Navier-Stokes equations, Comput. Methods Appl. Mech. Eng. 17/18 (1979) 673–689, Finite element penalty function approach
[7] M. Kawahara, On finite-element methods in shallow-water long-wave flow analysis, in: J.T. Oden (Ed.), Computational Methods in Nonlinear Mechanics, NorthHolland, Amsterdam, 1980, pp. 261–287.
[8] I.M. Navon, A review of finite element methods for solving the shallow water equations, Computer Modelling in Ocean Engineering, Balkema, Rotterdam, 1988, pp. 273–278.
[9] J.J. Connor, C.A. Brebbia, Finite-Element Techniques for Fluid Flow, Newnes-Butterworth, London and Boston, 1976.
[10] J.J. O'Brien, H.E. Hulburt, A numerical model of coastal upwelling, J. Phys. Oceanogr. 2 (1972) 14–26.
[11] M. Crepon, M.C. Richez, M. Chartier, Effects of coastline geometry on upwellings, J. Phys. Oceanogr. 14 (1984) 365–382.
[12] M.G.G. Foreman, An analysis of two-step time-discretisations in the solution of the linearized shallow-water equations, J. Comput. Phys. 51 (1983) 454–483.
[13] W.R. Gray, D.R. Lynch, Finite-element simulation of shallow-water equations with moving boundaries, in: A. Brebbia et al. (Eds.), Proceedings of 2nd Conference on Finite-Elements in Water Resources, 1978, pp. 23–42.

[14] T.D. Malone, J.T. Kuo, Semi-implicit finite-element methods applied to the solution of the shallow-water equations, J. Geophys. Res. 86 (1981) 4029–4040.
[15] G.J. Fix, Finite-element models for ocean-circulation problems, SIAM J. Appl. Math. 29 (1975) 371–387.
[16] C. Taylor, J. Davis, Tidal and long-wave propagation, a finite-element approach, Comput. Fluids 3 (1975) 125–148.
[17] M.J.P. Cullen, A simple finite element method for meteorological problems, J. Inst. Math. Appl. 11 (1973) 15–31.
[18] H.H. Wang, P. Halpern, J. Douglas Jr., I. Dupont, Numerical solutions of the one-dimensional primitive equations using Galerkin approximations with localised basis functions, Mon. Weekly Rev. 100 (1972) 738–746.
[19] I.M. Navon, Finite-element simulation of the shallow-water equations model on a limited area domain, Appl. Math. Modell. 3 (1979) 337–348.
[20] M.J.P. Cullen, The finite element method, in: Numerical Methods Used in Atmosphere Models, WMO/GARP Publication Series, vol. 7, World Meteorological Organisation, Geneva, Switzerland, 1979, pp. 330–338.
[21] M.J.P. Cullen, C.D. Hall, Forecasting and general circulation results from finite-element models, Q. J. Roy. Met. Soc. 102 (1979) 571–592.
[22] D.E. Hinsman, R.T. Williams, E. Woodward, Recent advances in the Galerkin finite-element method as applied to the meteorological equations on variable resolution grids, in: T. Kawai (Ed.), Finite-Element Flow-Analysis, University of Tokyo Press, Tokyo, 1982.
[23] I.M. Navon, A Numerov-Galerkin technique applied to a finite-element shallow-water equations model with enforced conservation of integral invariants and selective lumping, J. Comput. Phys. 52 (1983) 313–339.
[24] I.M. Navon, R. de Villiers, Gustaf, a quasi-Newton nonlinear ADI FORTRAN IV program for solving the shallow-water equations with augmented lagrangians, Comput. Geosci. 12 (1986) 151–173.
[25] A.N. Staniforth, A review of the application of the finite-element method to meteorological flows, in: T. Kawai (Ed.), Finite-Element Flow-Analysis, University of Tokyo Press, Tokyo, 1982, pp. 835–842.
[26] A.N. Staniforth, The application of the finite element methods to meteorological simulations—a review, Int. J. Numer. Methods Fluids 4 (1984) 1–22.
[27] R.T. Williams, O.C. Zienkiewicz, Improved finite element forms for shallow-water wave equations, Int. J. Numer. Methods Fluids 1 (1981) 91–97.
[28] M.G.G. Foreman, A two-dimensional dispersion analysis of selected methods for solving the linearised shallow-water equations, J. Comput. Phys. 56 (1984) 287–323.
[29] I.M. Navon, FEUDX: A two-stage, high-accuracy, finite-element FORTRAN program for solving shallow-water equations, Comput. Geosci. 13 (1987) 225–285.
[30] P. Bettess, C.A. Fleming, J.C. Heinrich, O.C. Zienkiewicz, D.I. Austin, A numerical model of longshore patterns due to a surf zone barrier, in: A Numerical Model of Longshore Patterns Due to a Surf Zone Barrier, Hamburg, Germany, 1978.

[31] N. Takeuchi, M. Kawahara, T. Yoshida, Two step explicit finite element method for tsunami wave propagation analysis, Int. J. Numer. Methods Eng. 12 (1978) 331–351.
[32] J.H.S. Lee, J. Peraire, O.C. Zienkiewicz, The characteristic Galerkin method for advection dominated problems—an assessment, Comput. Methods Appl. Mech. Eng. 61 (1987) 359–369.
[33] D.R. Lynch, W. Gray, A wave equation model for finite element tidal computations, Comput. Fluids 7 (1979) 207–228.
[34] O. Daubert, J. Hervouet, A. Jami, Description on some numerical tools for solving incompressible turbulent and free surface flows, Int. J. Numer. Methods Eng. 27 (1989) 3–20.
[35] G. Labadie, S. Dalsecco, B. Latteaux, Resolution des équations de Saint-Venant par une méthode d'éléments finis, Electricité de France, Report HE/41, 1982.
[36] T. Kodama, T. Kawasaki, M. Kawahara, Finite element method for shallow water equation including open boundary condition, Int. J. Numer. Methods Fluids 13 (1991) 939–953.
[37] S. Bova, G. Carey, An entropy variable formulation and applications for the two dimensional shallow water equations, Int. J. Numer. Methods Fluids 23 (1996) 29–46.
[38] K. Kashiyama, H. Ito, M. Behr, T. Tezduyar, Three-step explicit finite element computation of shallow water flows on a massively parallel computer, Int. J. Numer. Methods Fluids 21 (1995) 885–900.
[39] S. Chippada, C. Dawson, M. Martinez, M.F. Wheeler, Finite element approximations to the system of shallow water equations, SIAM J. Numer. Analysis 35 (1998) 692–711, Part I. Continuous time a priori error estimates. TICAM Report, Univ. of Texas at Austin
[40] S. Chippada, C. Dawson, M. Martinez, M.F. Wheeler, Finite element approximations to the system of shallow water equations, SIAM J. Numer. Analysis 36 (1998) 226–250, Part II. Discrete time a priori error estimates. TICAM Report, Univ. of Texas at Austin
[41] O.C. Zienkiewicz, J. Wu, J. Peraire, A new semi-implicit or explicit algorithm for shallow water equations, Math. Mod. Sci. Comput. 1 (1993) 31–49.
[42] M.M. Cecchi, L. Salasnich, Shallow water theory and its application to the Venice lagoon, Comput. Methods Appl. Mech. Eng. 151 (1998) 63–74.
[43] M.M. Cecchi, A. Pica, E. Secco, A projection method for shallow water equations, Int. J. Numer. Methods Fluids 27 (1998) 81–95.
[44] F.X. Giraldo, The Lagrange-Galerkin method for the two-dimensional shallow water equations on adaptove grids, Int. J. Numer. Methods Fluids 33 (2000) 789–832.
[45] C.N. Dawson, M.L. Martinez-Canales, A characteristic-Galerkin approximation to a system of shallow water equations, Numer. Math. 86 (2000) 239–256.
[46] V. Aizinger, C. Dawson, A discontinuous Galerkin method for two-dimensional flow and transport in shallow water, Adv. Water Resour. 25 (2002) 67–84.

[47] C. Dawson, J. Proft, Discontinuous and coupled continuous/discontinuous Galerkin methods for the shallow water equations, Comput. Methods Appl. Mech. Eng. 191 (2002) 4721–4746.
[48] M. Quecedo, M. Pastor, A reappraisal of Taylor-Galerkin algorithm for drying-wetting areas in shallow water computations, Int. J. Numer. Methods Eng. 38 (2002) 515–532.
[49] F.X. Giraldo, Strong and weak Lagrange-Galerkin spectral methods for the shallow water equations, Comput. Math. Appl. 45 (2003) 97–121.
[50] C. Dawson, J. Proft, Discontinuous/continuous Galerkin methods for coupling the promitive and wave continuity equations of shallow water, Comput. Methods Appl. Mech. Eng. 192 (2003) 5123–5145.
[51] C. Dawson, J. Proft, Coupled discontinuous and continuous Galerkin finite element methods for the depth integrated shallow water equations, Comput. Methods Appl. Mech. Eng. 193 (2004) 289–318.
[52] M. Morandi-Cecchi, M. Venturin, Characteristic-based split (CBS) algorithm finite element modelling for shallow waters in the Venice lagoon, Int. J. Numer. Methods Eng. 66 (2006) 1641–1657.
[53] V. Rostand, D.Y. Le Roux, Raviart-Thomas and Brezzi-Douglas-Marini finite-element approximations of the shallow-water equations, Int. J. Numer. Methods Fluids 57 (8) (2008) 951–976.
[54] D.Y. Le Roux, E. Hanert, V. Rostand, B. Pouliot, Impact of mass lumping on gravity and Rossby waves in 2D finite-element shallow-water models, Int. J. Numer. Methods Fluids 59 (7) (2009) 767–790.
[55] R. Comblen, J. Lambrechts, J.-F. Remacle, V. Legat, Practical evaluation of five partly discontinuous finite element pairs for the non-conservative shallow water equations, Int. J. Numer. Methods Fluids 63 (6) (2010) 701–724.
[56] D.Y. Le Roux, R. Walters, E. Hanert, J. Pietrzak, A comparison of the GWCE and mixed P-P1 formulations in finite-element linearized shallow-water models, Int. J. Numer. Methods Fluids 68 (12) (2012) 1497–1523.
[57] C.J. Trahan, C. Dawson, Local time-stepping in Runge-Kutta discontinuous Galerkin finite element methods applied to the shallow-water equations, Comput. Methods Appl. Mech. Eng. 217 (2012) 139–152.
[58] O.C. Zienkiewicz, P. Ortiz, A split characteristic based finite element model for shallow water equations, Int. J. Numer. Methods Fluids 20 (1995) 1061–1080.
[59] O.C. Zienkiewicz, P. Ortiz, The CBS (characteristic-based-split) algorithm in hydraulic and shallow water flow, in: Second International Symposium River Sedimentation and Environment Hydraulics, University of Hong Kong, December 1998, pp. 3–12.
[60] O.C. Zienkiewicz, R. Codina, A general algorithm for compressible and incompressible flow—Part I: The split, characteristic-based scheme, Int. J. Numer. Methods Fluids 20 (1995) 869–885.
[61] R. Löhner, K. Morgan, O.C. Zienkiewicz, The solution of non-linear hyperbolic equation systems by the finite element method, Int. J. Numer. Methods Fluids 4 (1984) 1043–1063.

[62] S. Nakazawa, D.W. Kelly, O.C. Zienkiewicz, I. Christie, M. Kawahara, An analysis of explicit finite element approximations for the shallow water wave equations, in: Proceedings of the 3rd International Conference on Finite Elements in Flow Problems, Banff, vol. 2, 1980, pp. 1–7.
[63] M. Kawahara, H. Hirano, K. Tsubota, K. Inagaki, Selective lumping finite element method for shallow water flow, Int. J. Numer. Methods Fluids 2 (1982) 89–112.
[64] D.R. Lynch, W.G. Gray, Analytic solutions for computer flow model testing, Trans. ASCE 104 (1978) 1409–1428, J. Hydr. Div. (10)
[65] Hydraulic Research Station, Severn tidal power, Report EX985, 1981.
[66] D.I. Austin, P. Bettess, Longshore boundary conditions for numerical wave model, Int. J. Numer. Mech. Fluids 2 (1982) 263–276.
[67] C.K. Ziegler, W. Lick, The transport of fine grained sediments in shallow water, Environ. Geol. Water Sci. 11 (1988) 123–132.